Comparison of Emeralds from the Chitral District, Pakistan, with other Pakistani and Afghan Emeralds

Carina S. Hanser, Tom Stephan, Bilal Gul, Tobias Häger and Roman Botcharnikov

ABSTRACT: Emeralds from various deposits in Pakistan (Chitral, Swat and Khaltaro) and Afghanistan (Panjshir and Laghman) were examined and compared. In addition, we compared the lighter-coloured Chitral emeralds from our previous study to newly acquired, more deeply coloured samples from Chitral. The specimens were characterised by Raman, FTIR and UV-Vis-NIR spectroscopy. Chemical analyses by EPMA and LA-ICP-MS also were performed on the samples from Chitral and Khaltaro. Distinguishing features of our Chitral emeralds include a lack of three-phase inclusions, a strong Fe^{2+}-related absorption at about 830 nm in the UV-Vis-NIR spectra, and elevated Cs and Li contents. These characteristics may provide clues for geographic origin determination.
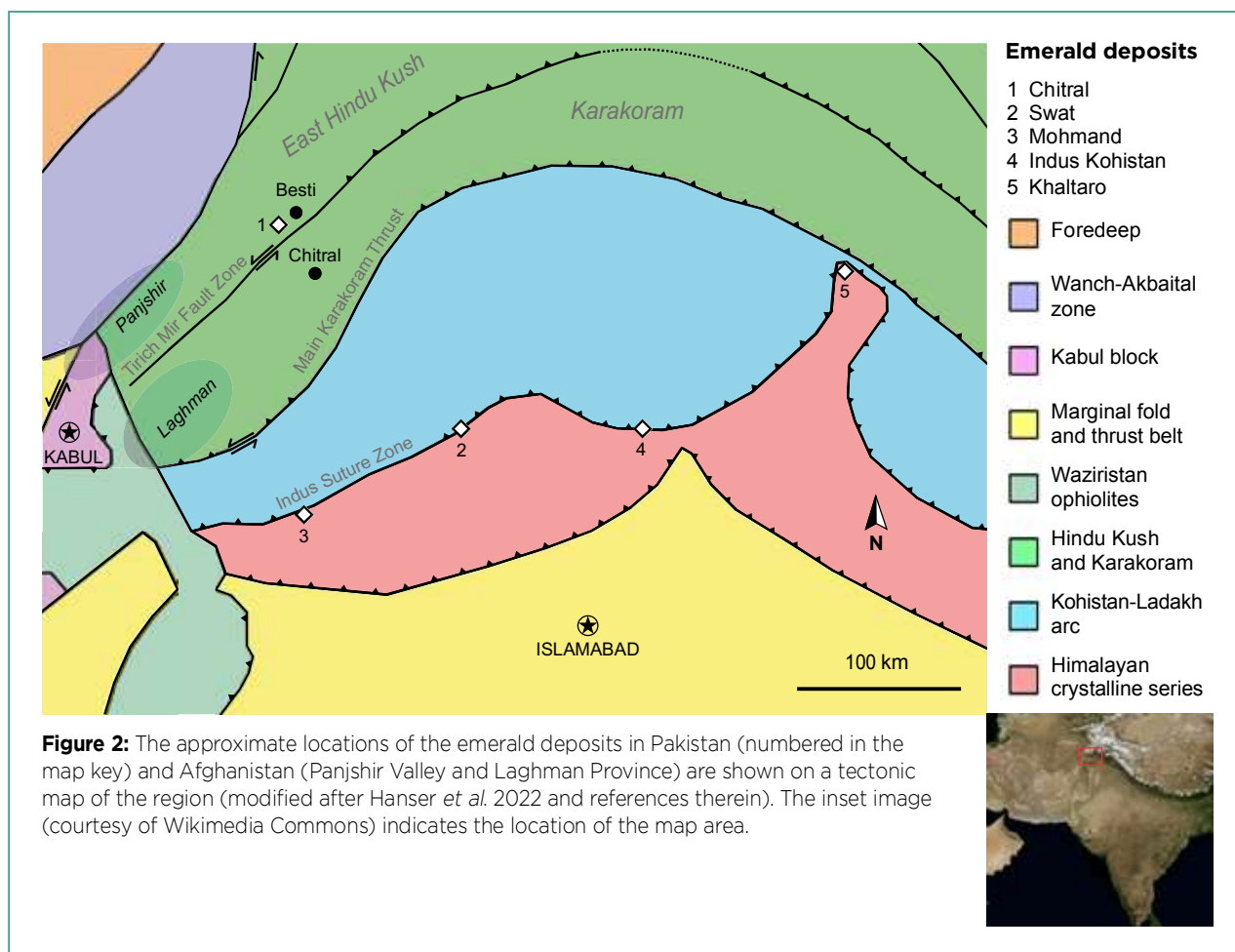
Emeralds from Pakistan and Afghanistan have most likely been known for thousands of years. It is widely recognised today that the so-called Bactrian emeralds from old Hindu treasures (around 1000 CE) may have originated from mines in Afghanistan and Pakistan (Schwarz & Curti 2021). Giuliani *et al.* (2000) determined the oxygen isotopic composition of an emerald set in a Gallo-Roman earring, which exhibited an isotopic signature known only from emeralds of the Swat Valley in Pakistan. This discovery is seen as proof that mining in this region has taken place since antiquity. Yet, new deposits continue to be found there, including the recent discovery in 2021 of emeralds in the Chitral District of north-western Pakistan (Hanser *et al.* 2022; see, e.g., Figure 1 and the cover of this issue).

During the late 1950s to mid-1960s, emeralds were rediscovered in the Swat and Mohmand districts of Pakistan (Kazmi & Snee 1989; Lawrence *et al.* 1989).

Figure 1: Gem-quality emeralds were recently discovered in the Chitral District of north-western Pakistan. This specimen of Chitral emerald crystals on a mica matrix weighs approximately 1.25 kg. Photo by Waqar Ahmed.

Figure 2: The approximate locations of the emerald deposits in Pakistan (numbered in the map key) and Afghanistan (Panjshir Valley and Laghman Province) are shown on a tectonic map of the region (modified after Hanser *et al.* 2022 and references therein). The inset image (courtesy of Wikimedia Commons) indicates the location of the map area.

These deposits are limited to a narrow tectonic zone—the Indus suture zone (Figure 2), often also referred to as the 'emerald belt' (Lawrence *et al.* 1989)—in which melanges of various oceanic rocks provided the necessary Cr and V for the genesis of emeralds (Kazmi 1989; Lawrence *et al.* 1989; Snee *et al.* 1989). The later discovery (in 1985) of emeralds near Khaltaro in the Haramosh mountains—where pegmatites and hydro-thermal veins intruded amphibolite—represent the first Pakistani findings outside the 'emerald belt' (Laurs *et al.* 1996). According to previous work, Pakistani emeralds from Swat, Mohmand and Khaltaro show differences in their chemical compositions, possibly serving as fingerprints for these localities (Snee *et al.* 1989). Further detailed studies of emeralds from Afghanistan and Pakistan have been published in recent years (e.g. Krzemnicki *et al.* 2021; Hanser *et al.* 2022). These studies include the tectonic-metasomatic deposits of the Panjshir Valley and the likely metabasite-related Laghman emeralds, both in Afghanistan (Giuliani *et al.* 2019; Krzemnicki *et al.* 2021).

Emeralds from the new deposit near Chitral in Pakistan occur in veins within quartz- and mica-rich host rocks of the Hindu Kush mountains (Hanser *et al.* 2022). The majority of this region consists of the metapelites of the Arkari Formation, which was intruded by dykes and plutons of pegmatitic leuco-granite (Khan 1986; Zahid *et al.* 2016). The remoteness and altitude of the deposit only allow limited access to the mining area by a narrow road. In 2022 this road, which previously ended several hundred metres from the mine, was extended to the mining site itself. This enabled the transport of machines to the emerald workings. Despite the strongest monsoon season in a decade, production increased from 130 kg of loose emerald in 2021 to over 300 kg in 2022.

The previous study by Hanser *et al.* (2022) mainly focused on comparing Chitral emeralds to those from the most important global localities, but some similarities of light-coloured Chitral samples to emeralds from other deposits in Afghanistan and Pakistan were established. However, the Chitral deposit also produces emeralds of more intense colour (Figure 3). This follow-up study characterises these more deeply coloured Chitral emeralds and compares them to those of other Pakistani and Afghan deposits. The main goal

Figure 3: Chitral produces emeralds with sufficiently saturated colour, such as this 11.25 ct cushion-cut stone, to make it a potentially important source for the gem market. Photo by Anne Fulton; courtesy of Dudley Blauwet Gems.

is to differentiate emeralds from these occurrences based on their physical, chemical and microscopic characteristics in order to identify features that are helpful for origin determination.

MATERIALS AND METHODS

Samples

For this study, a total of 32 emeralds were examined (Table I and Figure 4). They consisted of 22 Pakistani samples (six from Chitral, two from Khaltaro and 14 from the Swat District), and ten specimens from Afghanistan (two from Laghman Province and eight from the Panjshir Valley). The emeralds from the various mining areas in the Swat District—including two from Charbagh, four from Gujar Killi, three from Makhad and five of unspecified origin—proved to show insignificant differences, so these samples are lumped together under 'Swat' in this study. The samples from Swat, Laghman and Panjshir came from the reference collection of the German Gemmological Association. The Khaltaro specimens used in this study were obtained from old stock, since mining of this locality has ceased almost entirely. The Chitral emeralds were supplied by mine owner Imran Khan.

Small slices from each of the Chitral and Khaltaro emeralds were cut and polished with their faces oriented parallel to the *c*-axis, as described by Hanser *et al.* (2022). The Swat samples had been previously polished into plates with two surfaces parallel to the *c*-axis. One of the Panjshir samples consisted of a crystal which contained some parallel faces, while the other seven Panjshir samples—and the two from Laghman—were faceted with the *c*-axis oriented parallel to the table facet.

Analyses of Chitral and Khaltaro Emeralds

The Chitral and Khaltaro emeralds were analysed at Johannes Gutenberg-University (Mainz, Germany). Refractive indices were measured with a standard refractometer and SG was determined hydrostatically. A Leica microscope was used to examine internal features. The optical path was vertical and photos were taken with an attachable camera unit.

For ultraviolet-visible-near infrared (UV-Vis-NIR), Fourier-transform infrared (FTIR) and Raman spectroscopy, polarised spectra were recorded in two directions, with the electric field vector E of the incident light being perpendicular (E⊥c) and parallel (E∥c) to the *c*-axis. While all of the Chitral emeralds were analysed with the various spectroscopic methods, only one Khaltaro sample was transparent enough to allow UV-Vis-NIR and FTIR analyses to be performed. Details of the analysis parameters for the different techniques and instruments can be found in Hanser *et al.* (2022). However, for UV-Vis-NIR spectroscopy the acquisition times for the UV and NIR ranges were increased to 222 ms and 250 ms, respectively, to compensate for the decreasing output of an ageing light source.

The Chitral and Khaltaro emeralds were chemically analysed at Johannes Gutenberg-University by electron probe micro-analysis (EPMA; six spots per sample) and laser ablation inductively coupled plasma mass spectrometry (LA-ICP-MS; five spots per sample). Details on the instruments and their operating conditions are provided by Hanser *et al.* (2022). The trace elements Cs and Rb were determined only with LA-ICP-MS. For EPMA, the samples were embedded in acrylic using ClaroCit (powder and liquid hardener). EPMA analyses of surface-reaching inclusions utilised different standards than the beryl analyses: calibrations on pollucite and metallic vanadium were not performed; wollastonite was used for Ca and Si, and α-Al_2O_3 was used for Al (rather than diopside and aluminosilicate, respectively).

Analyses of Swat, Laghman and Panjshir Emeralds

The Swat, Laghman and Panjshir emeralds were analysed in the laboratories of the German Gemmological Association and the DSEF German Gem Lab in Idar-Oberstein, Germany. Refractive indices were measured with a standard refractometer using a contact liquid with

Table I: Emerald samples examined for this study.

Sample*	Colour	Diaphaneity	Dimensions (mm)	Weight (ct)
Chi8	Medium green	Transparent	9.06 × 11.95 × 3.17	2.959
Chi9	Dark green	Transparent (except for mica cluster)	5.42 × 9.44 × 4.09	2.272
Chi10	Medium green	Transparent	9.65 × 6.49 × 3.08	1.533
Chi11	Medium green	Transparent	10.03 × 6.54 × 3.51	1.775
Chi12	Medium green	Transparent	8.62 × 7.97 × 3.79	2.777
Chi13	Light green	Transparent	8.61 × 9.55 × 5.35	4.429
Kha1	Pale green	Translucent	6.95 × 6.81 × 2.98	1.177
Kha2	Pale green	Slightly translucent, almost opaque	9.14 × 8.02 × 2.64	1.433
Lag1	Intense green	Semi-transparent	10.59 × 10.55 × 3.98	3.546
Lag2	Dark green	Semi-transparent	11.28 × 9.03 × 3.92	2.991
Pan1	Green	Transparent	6.59 × 6.46 × 5.50	1.935
Pan2	Green	Transparent	3.07 × 3.03 × 1.91	0.122
Pan3	Green	Transparent	3.14 × 3.12 × 1.89	0.133
Pan4	Green	Transparent	4.22 × 2.74 × 1.68	0.148
Pan5	Green	Transparent	3.24 × 3.21 × 1.93	0.155
Pan6	Light green	Transparent	4.47 × 2.99 × 1.73	0.186
Pan7	Green	Transparent	3.53 × 3.52 × 2.20	0.204
Pan8	Green	Transparent	5.70 × 3.33 × 2.29	0.361
Swat1	Intense green	Transparent	3.50 × 2.58 × 1.05	0.087
Swat2	Intense green	Transparent	3.35 × 2.95 × 1.28	0.107
Swat3	Intense green	Translucent	4.03 × 2.75 × 1.58	0.138
Swat4	Intense green	Transparent	3.20 × 2.27 × 1.20	0.089
Swat5	Intense green	Transparent	2.90 × 2.64 × 1.55	0.111
Swat6	Pale green	Transparent (except for clusters of dark inclusions)	5.15 × 3.61 × 1.40	0.208
Swat7	Pale green	Transparent	3.32 × 2.90 × 1.55	0.128
Swat8	Pale green	Transparent	3.20 × 3.04 × 1.22	0.094
Swat9	Pale green	Translucent	3.07 × 2.55 × 2.01	0.170
Swat10	Green	Translucent	2.61 × 1.98 × 1.28	0.060
Swat11	Intense green	Transparent	2.86 × 2.39 × 1.80	0.105
Swat12	Intense green	Transparent	2.21 × 2.08 × 1.36	0.061
Swat13	Intense green	Translucent	2.43 × 1.97 × 1.59	0.069
Swat14	Intense green	Transparent	2.36 × 2.23 × 1.16	0.047

* Chi = Chitral, Pakistan; Kha = Khaltaro, Pakistan; Lag = Laghman, Afghanistan; Pan = Panjshir Valley, Afghanistan; Swat = Swat District, Pakistan.

n = 1.780. Specific gravity was determined hydrostatically. Internal features were examined using a Schneider gemmological microscope with Zeiss Stemi2000 optics.

Optical absorption spectra were collected in both E⊥c and E||c directions with a PerkinElmer Lambda 950S UV-Vis-NIR spectrometer in the 200–2500 nm range, with a spectral resolution of 1 nm. Deuterium and tungsten halogen lamps were used as light sources. A detector change took place at 810 nm; longer wavelengths were recorded with an InGaAs detector, and shorter wavelengths with a photomultiplier tube.

In the 200–810 nm range the slit width was fixed at 4 nm, and for 810–2500 nm it was variable (2–4 nm). The device was equipped with an integration sphere to collect scattered light.

Infrared spectra were collected with a Magilabs GemmoFtir diffuse reflectance infrared Fourier transform (DRIFT) spectrometer. Polarisation is not possible with this device, so unpolarised spectra were recorded. Each sample was measured in the 400–7500 cm^{-1} range with 64 accumulations.

Raman spectroscopy of the emeralds was performed

using a Renishaw InVia Raman spectrometer with excitation in both $E{\perp}c$ and $E||c$ directions. The device was equipped with a 514 nm laser, a CCD detector and a grating with 1,200 lines/mm. The acquisition time was 10 s for each interval, and two accumulations were measured for each sample. The confocal analysis spot was focused slightly into the sample to avoid surface effects. Selected inclusions were identified with the same instrumentation using 514 and 785 nm lasers (and a grating with 1,800 lines/mm for the latter laser).

RESULTS

Sample Description

As with the previous Chitral emerald study (Hanser *et al.* 2022), the six Chitral samples examined here consisted of fragments of larger crystals, although some crystal faces were recognisable. In contrast to the previous study, the present Chitral samples were of higher quality, with a more saturated green colour and/or fewer inclusions (Figure 4a). Five of the emeralds were medium to dark green and only one sample (Chi13) was light green. Apart from a large mica cluster inclusion in Chi9, all six Chitral samples were transparent. However, the two Khaltaro samples were translucent to almost opaque (i.e. heavily included

and fractured; again, see Figure 4a). Although several pieces were sawn from the original rough sample Kha2, none were suitable for UV-Vis-NIR and FTIR analyses because the lack of diaphaneity did not allow enough light to be transmitted.

The samples from Panjshir, Laghman and Swat are shown in Figure 4b. All of the Panjshir samples were transparent. The crystal fragment (Pan1) was heavily included, but the faceted stones (Pan2–8) were quite clean. The Panjshir emeralds were mostly of a saturated green colour (some slightly yellowish). By contrast, the two faceted samples from Laghman were deeper green, semi-transparent and quite fractured. The Swat samples consisted of smaller, transparent to translucent fragments showing pale to intense green colouration (some slightly bluish). Some of the fragments were heavily included, particularly with eye-visible dark inclusions. One Swat sample (Swat5) was twinned.

Gemmological Properties and Inclusions

A summary of the gemmological properties and internal features in the study samples is provided in Table II. A variety of inclusions were present and some of them—such as partially healed fissures, hollow tubes, two-phase inclusions, carbonates and micas—were found to occur in samples from almost all of the localities.

Figure 4: The samples examined for this study consisted of: (**a**) six Chitral and two Khaltaro emeralds; and (**b**) reference emerald samples from the collection of the German Gemmological Association that originated from Laghman (two faceted stones), Panjshir (one crystal fragment and seven faceted stones) and the Swat District (14 polished fragments from various mining localities there). See Table I for the dimensions and weights of the stones. Photos by (**a**) C. S. Hanser and (**b**) T. Stephan.

Chitral. Two-phase inclusions in the Chitral samples were of a more-or-less rectangular to irregular shape (Figure 5a–d). The gas bubbles therein were mostly round, but some fluid inclusions contained more gas, which took up the majority of the space in these inclusions, thus causing the bubbles to become elongated (Figure 5d). Hollow tubes sometimes contained yellowish precipitates (Figure 5e, f). Although these solids could not be identified by Raman spectroscopy or EPMA, they may be iron hydroxides. One Chitral sample also contained a colourless rod-like crystal that reached the surface (Figure 5g), but it could not be analysed since it was on the side of the specimen that was mounted in acrylic. Fissures showing iridescent reflections were also seen (Figure 5h).

EPMA analyses of surface-reaching inclusions in the Chitral emeralds (Figure 6 and Table III) revealed that white, irregular crystal aggregates consisted of several mineral phases, including calcite, K-feldspar, plagioclase and quartz. The composition of plagioclase corresponded to oligoclase and andesine (cf. Deer *et al.* 2001), with CaO contents of approximately 3–8 wt.%. Darker inclusions were identified as phlogopite (Figure 6f, g). Only one mica inclusion analysed was consistent with the composition of muscovite (cf. Fleet 2003). Apart from phlogopite, no other dark mineral inclusions were present in the samples from Chitral.

Khaltaro. The Khaltaro samples contained many, mostly light-coloured, inclusions. White crystals typically consisted of calcite and albite (with less than 0.5 wt.% CaO; see Table III and Figure 7a). Mica was also present, with compositions corresponding to muscovite (Table III and Figure 7a; cf. Laurs *et al.* 1996). In addition, the Khaltaro samples contained altered, partly dissolved elongate crystal inclusions, some of which exhibited recognisable crystal faces (Figure 7b). Their appearance suggested an amphibole, but Raman spectroscopy and EPMA analyses identified them as muscovite.

Panjshir. The most common internal features in the Panjshir samples were fluid inclusions, which were present as partially healed fractures, isolated negative crystals (i.e. three-phase inclusions; Figure 8a, b) and hollow tubes (Figure 8c). The tubes were observed in all samples, always elongated parallel to the *c*-axis. The surface-reaching ones were sometimes filled with a yellowish brown substance (most likely iron hydroxides). The fluid inclusions in the Panjshir specimens contained two or three phases. In the larger ones especially, we observed the typical combination of a liquid, a gas and a solid (cubic) phase, as is also known to occur in Colombian emeralds. According to Bowersox *et al.* (1991), the three-phase inclusions in Panjshir emeralds contain up to eight daughter crystals, an H_2O-dominated liquid and CO_2 as the gaseous phase. The solid inclusions are most commonly halite (NaCl), but sometimes sylvite (KCl). Often, the three-phase inclusions were oriented along the *c*-axis and had rectangular shapes, but in other orientations they showed irregular shapes with jagged outlines.

The solid inclusions in our Panjshir emeralds consisted of irregular-shaped to well-formed rhombohedral carbonate inclusions (most likely calcite and/or dolomite), as well as colourless crystals, mostly in irregular shapes. Some were identified as quartz, others as feldspar. In addition, sample Pan1 hosted dark, opaque inclusions with a metallic lustre (Figure 8d). These were

Table II: Summary of the standard gemmological properties of the emeralds examined for this study.

| Locality	SG	RIs	Birefringence	Inclusions
Chitral, Pakistan	2.71–2.74	1.580–1.582 1.589–1.590	0.008–0.009	Quartz, calcite, plagioclase (andesine, oligoclase), K-feldspar, phlogopite, muscovite (minor amounts), two-phase inclusions, partially healed fissures, hollow tubes
Khaltaro, Pakistan	2.65–2.73	1.581–1.590	0.009	Calcite, plagioclase (almost pure albite), muscovite
Laghman, Afghanistan	2.77	1.584–1.592	0.008	Two- and three-phase inclusions, partially healed fissures, hollow tubes, mica (biotite), growth structures parallel to the *c*-axis
Panjshir, Afghanistan	2.70–2.78	1.578–1.586 1.585–1.593	0.008–0.009	Two- and three-phase inclusions (with serrated rims), partially healed fissures, hollow tubes, carbonates (probably calcite or dolomite), opaque cubes (probably pyrite), colourless crystals (quartz and feldspar), strong growth structures (both parallel and perpendicular to the *c*-axis)
Swat, Pakistan	2.73–2.78	1.582–1.593 1.590–1.602	0.008–0.009	Micas (probably biotite/phlogopite and muscovite), carbonates (probably calcite or dolomite), talc(?), two-phase (rarely three-phase) inclusions, liquid thin films, partially healed fissures, hollow tubes, colour zoning, black opaque minerals (probably spinel and/or pyrite)
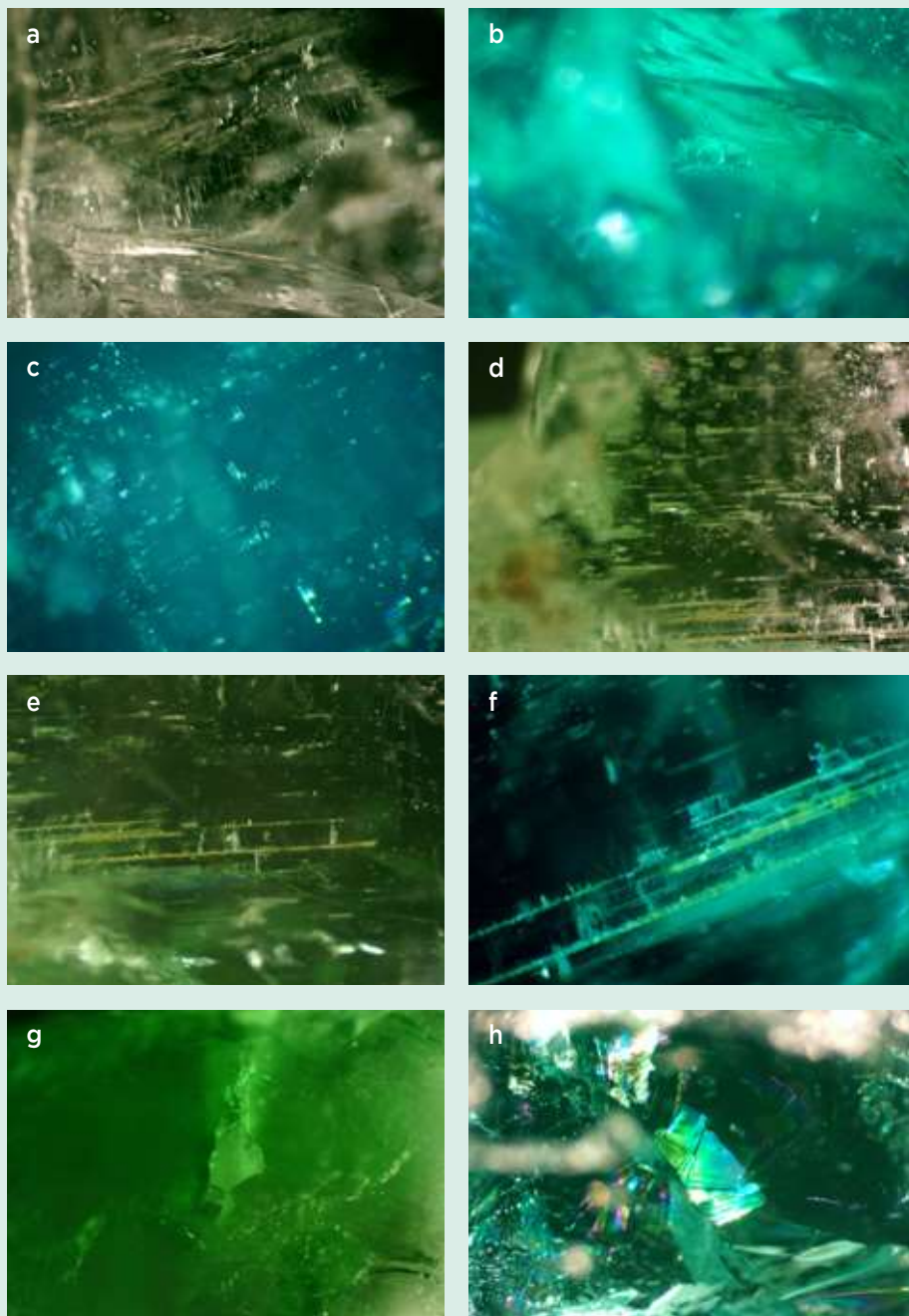
Figure 5: Inclusions found in the Chitral emeralds of this study include (**a**) partially healed fissures composed of two-phase fluid inclusions (sample Chi12; magnified 30×); (**b**) irregular two-phase fluid inclusions (Chi8; 100×); (**c**) rectangular two-phase fluid inclusions (Chi13; 100×); (**d**) thin, needle-like two-phase fluid inclusions with elongated gas bubbles and growth tubes (Chi13; 30×); (**e**) growth tubes (Chi13; 30×); (**f**) hollow tubes, partially filled with yellow precipitates, which may be iron hydroxides (Chi13; 100×); (**g**) a surface-reaching, rod-like, colourless crystal (Chi11; 30×); and (**h**) fissures showing bright iridescent reflections (Chi8; 30×). Photomicrographs by C. S. Hanser.

mostly irregularly shaped to rounded, and some had a subhedral cubic shape. They could not be identified by Raman spectroscopy because of a weak signal, but most likely consisted of pyrite (Bowersox *et al.* 1991; Schwarz & Pardieu 2009; Schwarz & Curti 2021).

Other internal features in the Panjshir samples included prominent growth structures parallel and perpendicular to the *c*-axis, often with typical 'sawtooth' structures.

Overall, our observations of the Panjshir emeralds are consistent with the literature (Bowersox *et al.* 1991; Moroz & Eliezri 1999; Sabot *et al.* 2001; Schwarz & Pardieu 2009; Schwarz & Curti 2021). However, these

authors additionally mentioned limonite, beryl, tourmaline and graphite inclusions.

Laghman. The two faceted Laghman emeralds possessed low transparency, particularly due to many cracks and fissures, as well as tiny liquid inclusions (Figure 9a). These same samples were also studied previously by Henn and Schmitz (2014), who identified flake-like doubly refractive mineral inclusions as micas in both stones (Figure 9b). EPMA analysis by Henn and Schmitz (2014) of one such surface-reaching inclusion identified it as biotite. Henn and Schmitz (2014) also reported
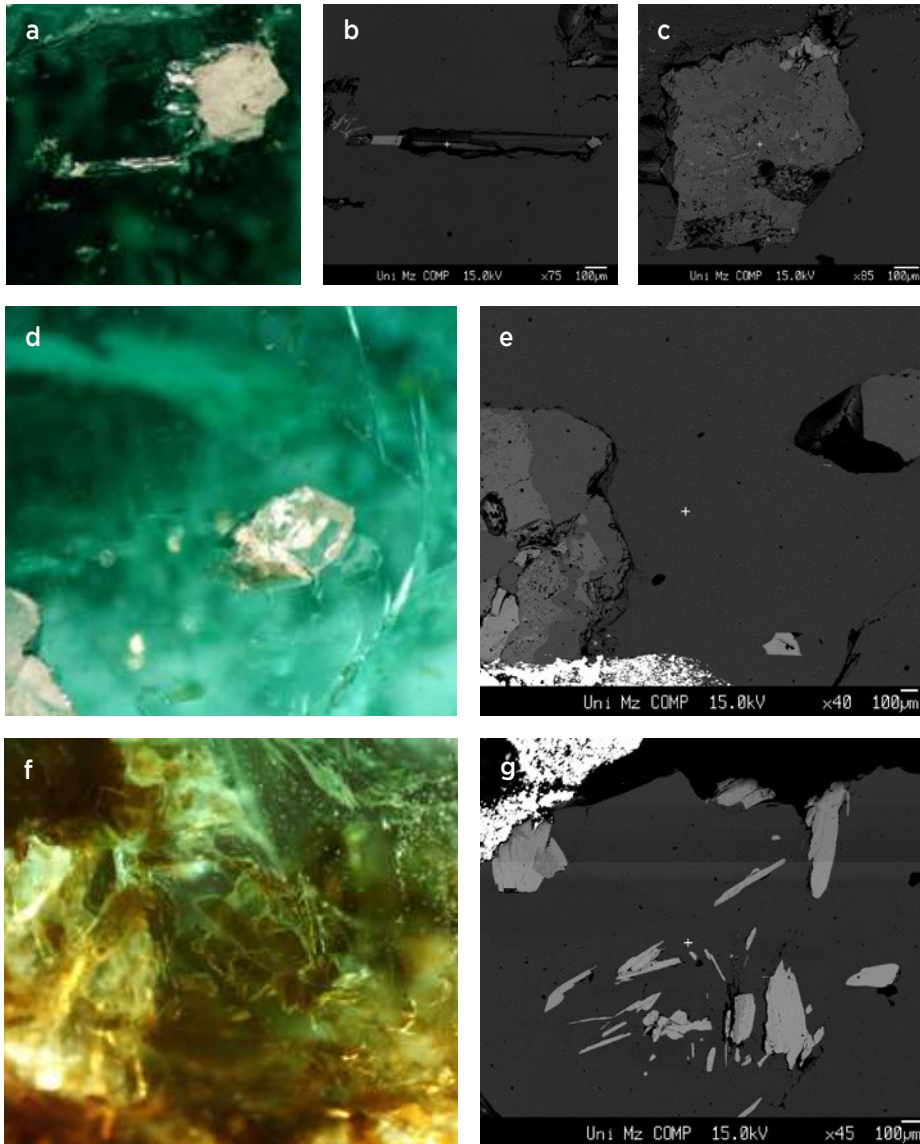
Figure 6: A number of surface-reaching inclusions were analysed by EPMA in the Chitral emeralds. (**a**) A rod-like crystal and a white, irregular inclusion were present in sample Chi8 (30×). Back-scattered electron (BSE) images obtained during EPMA analysis show (**b**) the rod-like crystal and (**c**) the irregular inclusion. The various grey tones seen in the irregular inclusion are due to differences in overall atomic weight corresponding to different mineral phases (identified as calcite, andesine, oligoclase and K-feldspar). (**d**) The colourless, partly euhedral crystal inclusion in the centre of this image of sample Chi8 was identified as quartz, while a cluster of inclusions at the lower left consists of quartz, andesine and K-feldspar (30×). (**e**) A BSE image is shown for a portion of the same area. The dark feature in the quartz crystal indicates where part of the crystal was plucked out during the cutting process. (**f**) A cluster of brown mica flakes is seen in Chi9 (30×). (**g**) A BSE image shows a similar cluster of mica (primarily phlogopite) in the same sample. Photomicrographs by C. S. Hanser and BSE images by N. Groschopf.

Table III: Representative EPMA analyses of inclusions in emeralds from Chitral and Khaltaro, Pakistan.[a]

Mineral	Oligoclase	Andesine	K-feldspar	Quartz	Calcite	Phlogopite	Muscovite	Albite	Muscovite
Sample no.	Chi8					Chi9		Kha2	
Oxide (wt.%)									
SiO_2	64.19	58.18	64.78	99.75	0.08	39.79	48.64	67.75	47.26
TiO_2	nd	nd	0.03	nd	0.04	0.64	0.12	nd	0.03
Al_2O_3	21.73	25.85	18.11	0.04	nd	14.33	28.24	19.48	29.95
Cr_2O_3	0.01	0.02	0.01	0.01	0.01	0.25	0.40	0.05	0.17
FeO	0.02	0.03	0.02	nd	0.11	9.83	0.66	0.04	1.76
MnO	0.01	0.02	nd	nd	nd	0.10	0.01	nd	0.31
MgO	0.01	nd	0.02	nd	0.05	18.00	2.86	nd	2.49
CaO	3.07	8.08	nd	nd	60.78	nd	nd	0.27	nd
Na_2O	9.98	7.33	0.05	nd	nd	0.32	0.27	11.66	0.30
K_2O	0.05	0.05	15.96	0.02	0.02	8.90	10.61	0.09	10.77
Total	99.07	99.57	98.99	99.83	61.10[b]	92.16[b]	91.81[b]	99.34	93.04[b]

[a] Abbreviation: nd = not detected.
[b] Total oxide content is low because CO_2, H_2O and possibly F cannot be determined by EPMA.
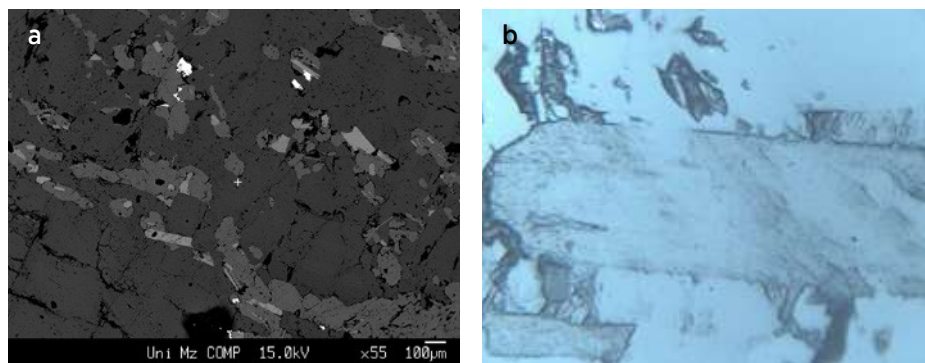
Figure 7: Various inclusions were analysed by EPMA in the Khaltaro emeralds. (**a**) This BSE image of Kha2 contains inclusions of mica, albite and calcite. (**b**) An elongated inclusion in Kha2 has an appearance that resembles an amphibole, but it was identified as muscovite (500×). Photomicrograph by C. S. Hanser and BSE image by N. Groschopf.

hollow tubes, rectangular two-phase negative crystals oriented parallel to the *c*-axis (Figure 9a) and partially healed fractures composed of tiny liquid droplets. In addition, Krzemnicki *et al.* (2021) mentioned amphibole (tremolite), mica (especially phlogopite) and graphite inclusions in Laghman emeralds.

In the present study, we identified no additional solid or liquid inclusions, except for yellowish brown substances in surface-reaching fissures and hollow tubes, again most likely iron hydroxides. The samples also showed prominent growth structures parallel to the *c*-axis.

Swat. The study samples from the Swat Valley were quite included, and all of them contained partially healed fractures composed of small liquid droplets which, in the larger ones, also contained a gas bubble. In addition, three-phase inclusions have been reported in Swat emeralds (Guo *et al.* 2020). Besides these fluid inclusions, larger

isolated two-phase negative crystals were also common in our samples, mainly with rectangular shapes parallel to the *c*-axis, but also showing irregular forms in other orientations. In addition, hollow tubes were observed.

The most common solid inclusions in the Swat emeralds were black opaque minerals (Figure 10), usually irregular in shape and with moderate-to-strong metallic lustre. They typically formed groups or were present as clouds. It was not possible to identify these inclusions with Raman spectroscopy due to their weak signal, but according to the literature they are most likely spinel and/or pyrite (Schwarz & Curti 2021). Flake-like mineral inclusions with strong double refraction were identified as mica. The colourless transparent ones were most likely muscovite, while the darker, brownish ones were probably biotite or phlogopite.

Irregularly shaped to partly rhombohedral transparent mineral inclusions were identified by Raman
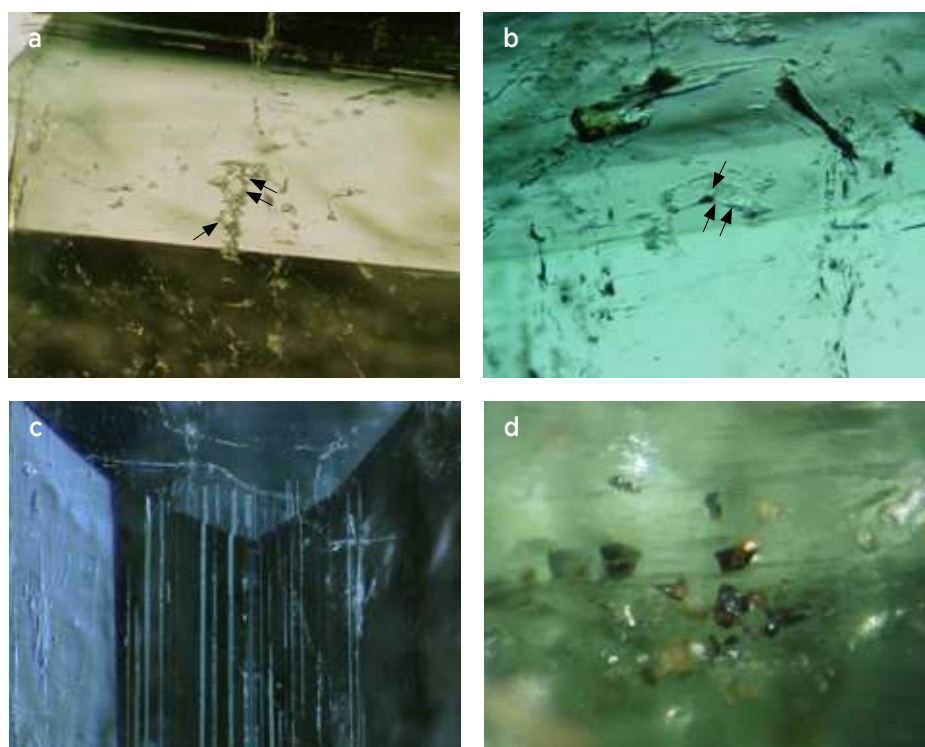

Figure 8: The Panjshir emeralds of this study exhibit both fluid and solid inclusions. (**a**, **b**) Sample Pan7 contains three-phase inclusions that each hosts three daughter crystals, which are marked by arrows (both 50×). (**c**) Hollow tubes are present in specimen Pan8 (40×). (**d**) Metallic inclusions, probably pyrite, are seen in sample Pan1 (50×). Photomicrographs by T. Stephan.
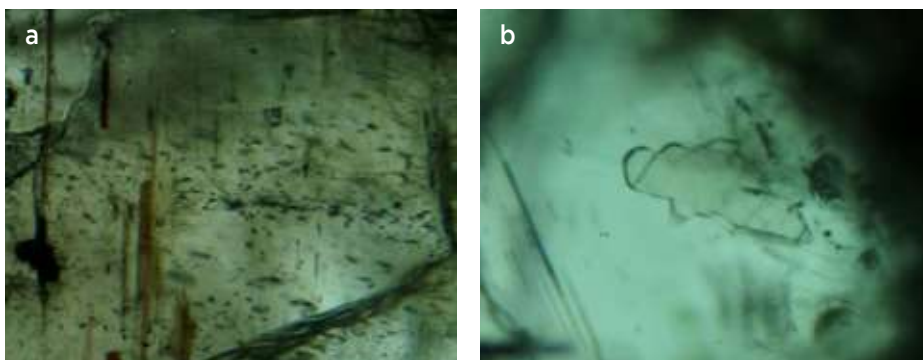
Figure 9: (**a**) Laghman emerald Lag2 contains abundant two-phase inclusions and brownish flakes that are most likely biotite (50×). (**b**) A mica inclusion is seen in Laghman sample Lag1 (40×); a similar inclusion was identified as biotite by Henn and Schmitz (2014). Photomicrographs by T. Stephan.

spectroscopy as carbonates, most likely calcite and/ or dolomite (cf. Gübelin 1982). Furthermore, some colourless to slightly greenish mineral inclusions were present, often as scaly to flaky crystals, and sometimes also irregularly distributed along fissures (Figure 10b). Owing to their small size and irregular distribution in fissures, these inclusions could not be identified by Raman spectroscopy, but they are most likely talc (cf. Gübelin & Koivula 2008; Schwarz & Curti 2021).

Growth lines were rarely observed in our Swat samples, but all showed weak-to-strong colour zoning, which was most obvious along the *c*-axis. Growth lines were previously described in Swat emeralds by Gübelin (1982) and by Schwarz and Curti (2021).

Our observations are consistent with the literature for Swat emeralds (Gübelin 1982; Gübelin & Koivula 2008; Schwarz & Curti 2021). Additional mineral inclusions documented by these other authors include actinolite, albite, magnesite, chlorite, chromite, enstatite, fuchsite, gersdorffite, plagioclase, pyrrhotite and quartz.

UV-Vis-NIR Spectroscopy

Figure 11 displays representative UV-Vis-NIR spectra (for the E⊥c direction) for emeralds from the various localities. (Spectra for the E||c direction are not shown since they are not as helpful for origin determination.) While all the samples exhibit V- and Cr-related absorptions, Fe-related features were noticeably stronger in some of them, especially those from Chitral and Laghman. The broad Fe^{2+} absorption around 830 nm is only weakly visible to absent in the emeralds from Panjshir and Swat (for the latter, regardless of the specific mine locality). Weaker absorption due to Fe^{2+} than to Cr^{3+} and V^{3+} is reported in the literature for emeralds from both Panjshir and Swat (Guo *et al.* 2020; Krzemnicki *et al.* 2021). By contrast, the Laghman emeralds showed similar to higher absorption intensities for Fe^{2+} compared to Cr^{3+} and V^{3+}, consistent with the literature (Krzemnicki *et al.* 2021). In the Chitral emeralds, the Fe^{2+} absorption was always stronger than the Cr^{3+} and V^{3+} features, which is consistent with previous findings (Hanser *et al.* 2022; see also the spectrum for sample PK1 in Figure 11).

Near-Infrared Spectroscopy

Representative near-infrared spectra of the Chitral and Khaltaro emeralds are shown in Figure 12. Several H_2O overtone peaks (Wood & Nassau 1967; Schmetzer & Kiefert 1990; Qiao *et al.* 2019; Hu & Lu 2020; Wang *et al.* 2022) are present in both the E||c and E⊥c spectra in the 6800–7300 cm^{-1} region (with fewer peaks in the E⊥c direction). In general, the patterns of these spectra agree with those of the lighter-coloured Chitral emeralds examined by Hanser *et al.* (2022), as can be seen by comparison with sample PK2 in Figure 12.

The same features were observed for the samples from Panjshir, Laghman and Swat, but those spectra were unpolarised and therefore are not shown for comparison.
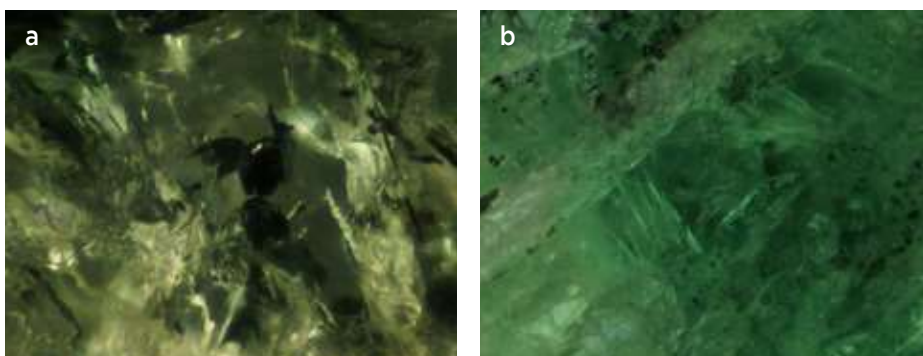

Figure 10: (**a**) Black and metallic inclusions, probably spinel and pyrite, respectively, are present in Swat emerald sample Swat5 (50×). (**b**) Emerald Swat12 contains a whitish vein (probably talc) and dark-appearing metallic inclusions (40×). Photomicrographs by T. Stephan.
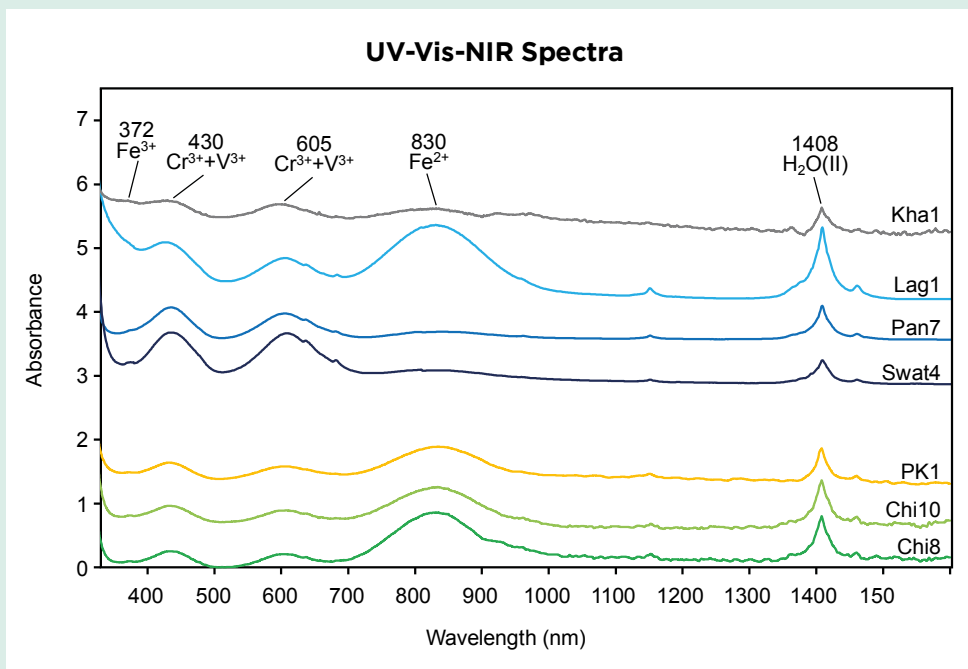
Figure 11:
Representative UV-Vis-NIR spectra (for E⊥c) for emeralds of this study are shown along with the spectrum of a Chitral sample (PK1) that was documented previously by Hanser *et al.* (2022). The spectra are offset vertically for clarity.
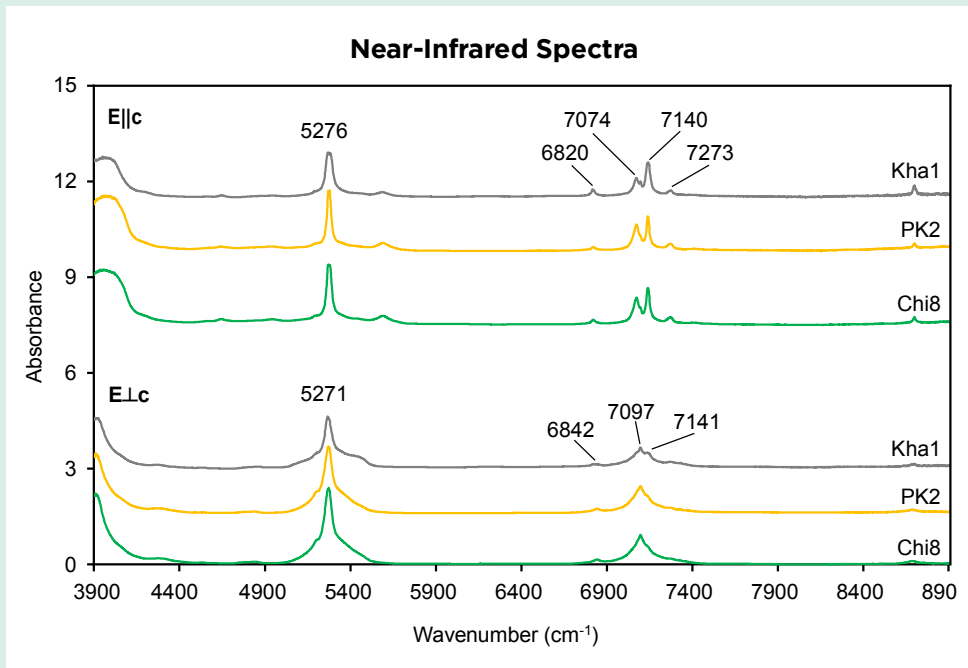

Figure 12:
Representative near-infrared spectra of emeralds from Chitral (Chi8) and Khaltaro (Kha1) are shown for both the E‖c and E⊥c directions. A representative spectrum of a lighter-coloured Chitral emerald (PK2) is provided for comparison (from Hanser *et al.* 2022). The spectra are offset vertically for clarity.

Raman Spectroscopy

For the E⊥c excitation direction (Figure 13a), in all the Chitral emerald samples the type I H_2O peak at a Raman shift of approximately 3608 cm^{-1} (Huong *et al*. 2010; Karampelas *et al*. 2019) was weaker than the type II H_2O peak at about 3598 cm^{-1} (Hagemann *et al*. 1990; Huong *et al*. 2010; Karampelas *et al*. 2019). This is consistent with our previous observations for lighter-coloured Chitral emeralds (see samples PK1 and PK7 in Figure 13a).

While the strength of these features was reversed in some Chitral samples for the E‖c direction (Figure 13b), the type I H_2O peak was stronger in both our Khaltaro samples, independent of the excitation direction. The Swat, Laghman and Panjshir emeralds also displayed strong type II water peaks (not shown here). This is in accordance with previous findings by Krzemnicki *et al*. (2021), who reported stronger type II water peaks for Laghman and some Panjshir emeralds.
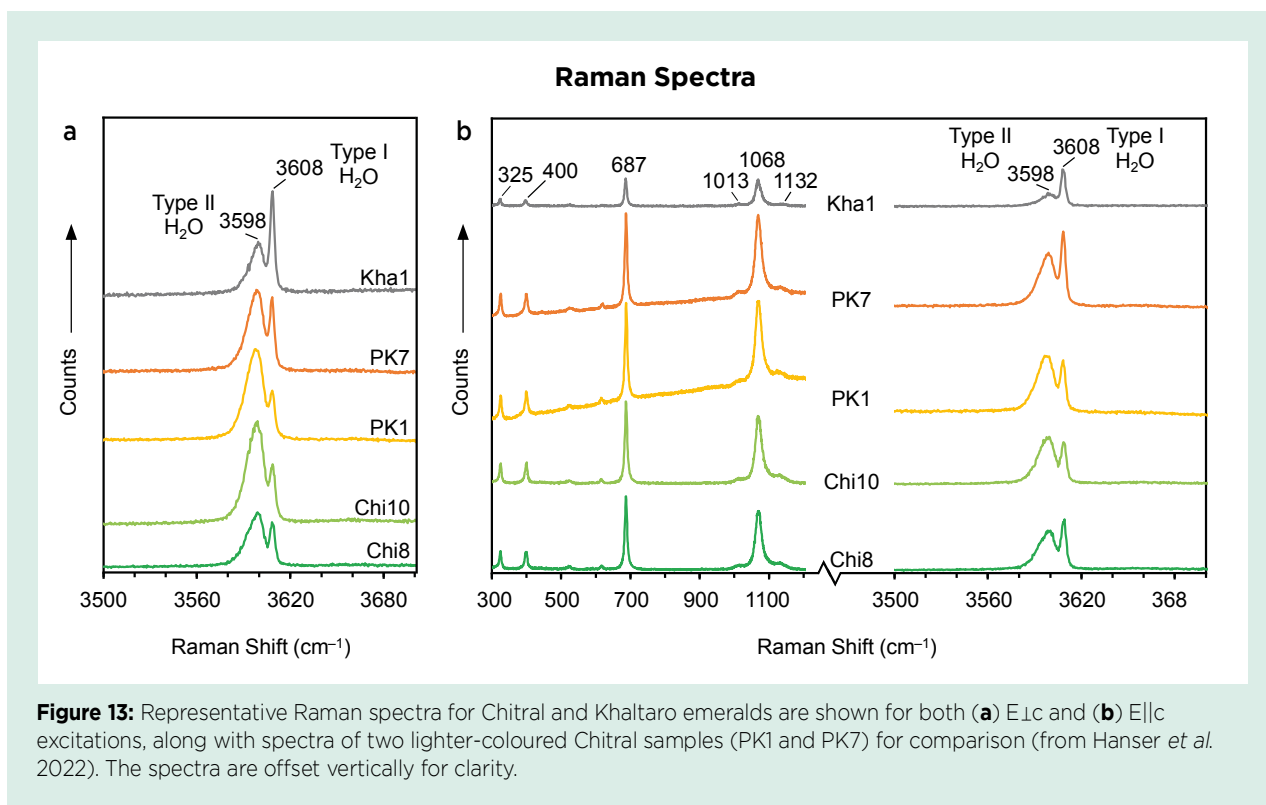
Figure 13: Representative Raman spectra for Chitral and Khaltaro emeralds are shown for both (**a**) E⊥c and (**b**) E∥c excitations, along with spectra of two lighter-coloured Chitral samples (PK1 and PK7) for comparison (from Hanser *et al.* 2022). The spectra are offset vertically for clarity.

Chemical Composition

Chemical analyses of the Chitral and Khaltaro emeralds by EPMA and LA-ICP-MS are summarised in Tables IV and V, respectively. In addition, *The Journal*'s online data depository contains all of the EPMA and LA-ICP-MS data obtained for this study (Tables DD-1 and DD-2, respectively), as well as all of the LA-ICP-MS analyses done by Hanser *et al.* (2022) on the previously examined Chitral emeralds (Table DD-3). Chemical plots from the EPMA and LA-ICP-MS data obtained for the present study, which also include analyses from the literature, are shown in Figures 14 and 15. For both analytical techniques, the chemical data for the Chitral emeralds in the present study are mostly in agreement with previous analyses reported by Hanser *et al.* (2022).

The contents of MgO and Na₂O show a positive correlation overall (Figure 14a). In general, lower concentrations of these elements are seen in Panjshir emeralds compared to those from Chitral, but they are enriched in Swat emeralds (Hammarstrom 1989; Aurisicchio *et al.* 2018). The contents of Mg and Na in the Laghman emeralds overlap those of Chitral (cf. Krzemnicki *et al.* 2021), and both of these elements were less abundant in the Khaltaro samples (Figure 14a and Table IV). In addition, some other common elements found in emerald—including Fe, Ca and V—were higher in the samples from Chitral than in those from Khaltaro. Concentrations of other elements—such as Li, K, Sc, Ti, Cr, Ga and Rb—overlapped between both localities, whereas Mn and Zn were at least twice as high in the Khaltaro emeralds. Concentrations of Fe overlap among emeralds from all the localities represented in this study (Figure 14b; see also Hammarstrom 1989 and Aurisicchio *et al.* 2018), except for the higher Fe values reported in Swat emeralds by Aurisicchio *et al.* (2018).

The Li contents of the Chitral samples were generally higher than in emeralds from all of the other Pakistani and Afghan localities except, in some cases, Khaltaro (Figure 15a; Guo *et al.* 2020; Krzemnicki *et al.* 2021; Chen *et al.* 2022). In addition, the Chitral emeralds showed notable Cs enrichment, generally exceeding the contents found in stones from the other localities considered in this study (except for Khaltaro in some cases; Figure 15b). Panjshir and Swat emeralds have low Cs values (Guo *et al.* 2020; Chen *et al.* 2022), but higher Cs contents are found in emeralds from Laghman (Krzemnicki *et al.* 2021). Similar trends apply to Rb (again, see Figure 15b; Guo *et al.* 2020; Krzemnicki *et al.* 2021; Chen *et al.* 2022). Overall, Cs shows a positive correlation with Rb for the analysed emeralds from Chitral, although not necessarily for the other localities.

The chromophores Cr and V also exhibited a positive correlation for the analysed stones from Chitral, but

Table IV: Average EPMA analyses of emeralds from Chitral and Khaltaro, Pakistan.[a]

Sample no.	Chi8	Chi9	Chi10	Chi11	Chi12	Chi13	Kha1	Kha2
Locality	Chitral						Khaltaro	
Oxide (wt.%)								
SiO_2	63.80	63.63	63.62	63.70	63.95	64.41	64.86	64.93
TiO_2	0.01	nd	nd	nd	nd	nd	nd	0.01
Al_2O_3	15.90	15.75	15.47	15.58	15.26	16.11	17.35	16.96
Cr_2O_3	0.12	0.17	0.11	0.12	0.10	0.09	0.08	0.23
V_2O_3	0.05	0.07	0.05	0.05	0.06	0.04	0.02	0.01
Fe_2O_3	0.57	0.54	0.59	0.63	0.54	0.50	0.27	0.41
BeO[b]	13.60	13.60	13.60	13.60	13.60	13.60	13.60	13.60
MgO	1.60	1.70	1.81	1.74	1.93	1.61	0.81	0.98
CaO	0.03	0.04	0.05	0.05	0.05	0.03	nd	nd
Na_2O	1.54	1.58	1.54	1.46	1.52	1.47	1.04	1.01
K_2O	0.04	0.04	0.06	0.05	0.06	0.03	0.03	0.04
H_2O[b]	0.85	0.85	0.85	0.85	0.85	0.85	0.85	0.85
Total	98.11	97.97	97.75	97.83	97.92	98.74	98.91	99.03
FeO[c]	0.51	0.48	0.53	0.57	0.49	0.45	0.24	0.37

[a] Averages are of six spots per sample. See *The Journal*'s online data depository for complete data. Abbreviation: nd = not detected.
[b] H_2O and BeO contents are fixed values, as commonly reported for beryl.
[c] The standard format for reporting Fe content in beryl by our instrument is Fe_2O_3, which is here recalculated to FeO.
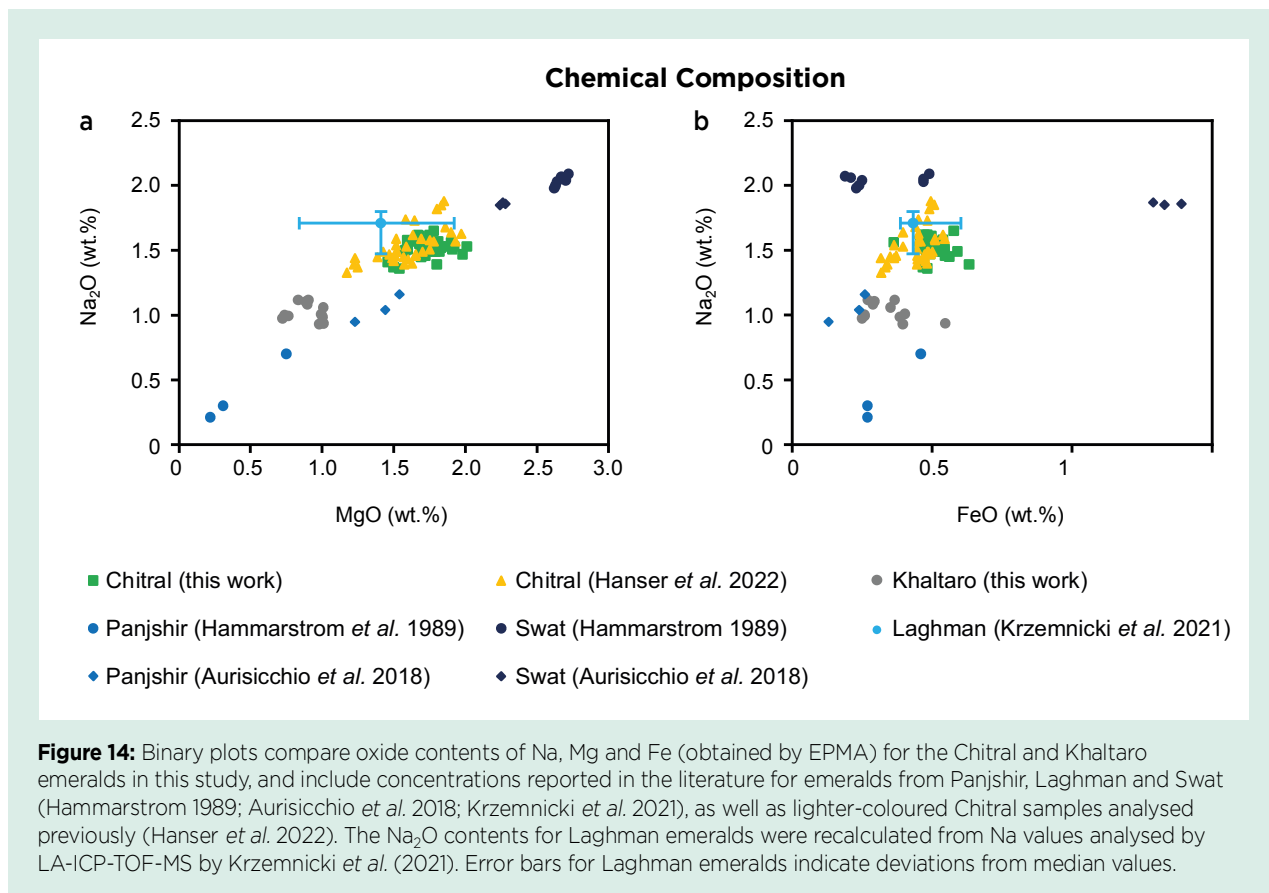

Figure 14: Binary plots compare oxide contents of Na, Mg and Fe (obtained by EPMA) for the Chitral and Khaltaro emeralds in this study, and include concentrations reported in the literature for emeralds from Panjshir, Laghman and Swat (Hammarstrom 1989; Aurisicchio *et al.* 2018; Krzemnicki *et al.* 2021), as well as lighter-coloured Chitral samples analysed previously (Hanser *et al.* 2022). The Na_2O contents for Laghman emeralds were recalculated from Na values analysed by LA-ICP-TOF-MS by Krzemnicki *et al.* (2021). Error bars for Laghman emeralds indicate deviations from median values.

Table V: Average LA-ICP-MS analyses of emeralds from Chitral and Khaltaro, Pakistan.*

Sample no.	Chi8	Chi9	Chi10	Chi11	Chi12	Chi13	Kha1	Kha2
Locality	Chitral						Khaltaro	
Element (ppm)								
Li	1133 (96.12)	1136 (37.49)	1231 (138.5)	1359 (80.70)	1309 (106.7)	938.7 (68.66)	940.7 (57.31)	677.6 (67.53)
Be	48080 (1567)	48330 (568.2)	47850 (871.2)	47350 (892.3)	46800 (568.8)	47500 (577.2)	47540 (1435)	48630 (710.2)
B	nd	1.56 (0.20)	2.16 (0.64)	nd	1.72 (0.28)	nd	nd	nd
Na	11490 (576.6)	11790 (197.6)	12040 (878.3)	10940 (359.8)	11530 (345.2)	11070 (617.5)	7434 (542.9)	7315 (386.4)
Mg	9188 (435.5)	9794 (184.3)	10640 (370.7)	10030 (566.9)	11140 (513.2)	9182 (602.8)	4407 (367.1)	5285 (809.0)
K	262.8 (20.32)	302.0 (4.89)	459.6 (43.76)	375.2 (23.75)	476.5 (25.19)	199.6 (15.64)	196.9 (30.69)	278.2 (612.50)
Ca	304.7 (67.74)	266.9 (61.05)	506.4 (38.32)	395.9 (104.3)	467.0 (67.66)	306.1 (55.21)	nd	nd
Sc	95.19 (3.95)	118.7 (4.35)	54.12 (3.47)	95.36 (3.50)	68.36 (3.54)	66.16 (15.14)	75.29 (13.14)	43.37 (25.12)
Ti	12.59 (3.21)	11.52 (1.54)	11.59 (0.77)	11.42 (1.47)	18.62 (1.61)	14.13 (1.82)	11.37 (5.48)	17.57 (6.53)
V	251.0 (14.54)	391.1 (8.21)	265.1 (14.24)	271.6 (17.55)	269.4 (15.46)	222.7 (15.65)	48.69 (13.10)	36.80 (16.82)
Cr	862.9 (46.34)	1197 (41.63)	779.0 (46.96)	858.4 (145.7)	590.3 (136.8)	514.9 (88.40)	659.7 (199.4)	1279 (276.5)
Mn	22.67 (2.83)	17.86 (0.72)	22.63 (1.59)	26.60 (1.37)	18.78 (1.52)	15.85 (1.82)	52.52 (3.26)	59.74 (28.32)
Fe	3876 (216.2)	3695 (135.1)	3965 (163.7)	4164 (213.0)	3659 (143.1)	3413 (301.5)	1789 (20.82)	2673 (107.5)
Co	1.83 (0.23)	1.79 (0.08)	1.76 (0.07)	1.73 (0.10)	1.52 (0.10)	1.54 (0.28)	nd	1.05 (0.18)
Ni	3.84 (1.50)	nd	2.49 (1.22)	nd	2.44 (0.61)	3.38 (1.78)	nd	13.21 (2.22)
Cu	nd	0.16 (0.03)	nd	0.12 (0.05)	nd	nd	nd	nd
Zn	18.47 (2.75)	12.95 (1.95)	14.65 (1.43)	15.15 (3.35)	13.20 (2.63)	17.78 (5.75)	45.41 (34.54)	32.13 (9.60)
Ga	15.80 (0.76)	13.06 (0.40)	8.65 (0.37)	11.44 (0.42)	6.79 (0.35)	12.49 (0.89)	10.53 (2.19)	9.51 (1.83)
Ge	nd	0.80 (0.19)	0.80 (0.22)	0.59 (0.08)	nd	nd	nd	nd
Rb	50.97 (6.29)	51.30 (1.74)	110.3 (3.71)	71.98 (7.16)	96.25 (2.43)	14.50 (1.54)	74.45 (5.01)	72.09 (3.74)
Y	nd	nd	nd	0.01 (0.01)	nd	nd	nd	nd
Zr	0.04 (0.01)	0.11 (0.18)	0.02 (0.02)	0.02 (0.004)	0.02 (0.02)	nd	nd	0.06 (0.04)
Sn	2.08 (1.36)	1.04 (0.38)	1.35 (0.37)	2.00 (0.55)	3.80 (0.46)	1.35 (0.43)	nd	0.81 (0.35)
Cs	3731 (167.3)	3486 (105.2)	5130 (113.4)	4190 (336.3)	5782 (233.5)	1151 (114.7)	2218 (254.21)	1366 (93.07)
Ba	nd	0.04 (0.01)	nd	nd	nd	nd	0.85 (0.67)	nd
Hf	nd	nd	nd	nd	0.01 (0.004)	nd	nd	nd
Tl	0.20 (0.08)	0.23 (0.05)	0.50 (0.07)	0.29 (0.04)	0.40 (0.05)	nd	0.95 (0.56)	0.40 (0.12)
U	0.01 (0.0004)	nd	nd	nd	nd	nd	nd	nd

* Averages are of five spots per sample, with corresponding standard deviations in parentheses. See *The Journal*'s online data depository for complete data. Abbreviation: nd = not detected.

this trend was not seen in the data for all of the other localities. (Figure 15c, d). The lighter Chitral emeralds have tended to have slightly lower concentrations of Cr and V, and the darkest sample of the previous study (PK1) showed similar contents of these elements as the Chitral emeralds analysed here. The Chitral samples showed higher V and overlapping Cr with those from Khaltaro, less Cr than emeralds from Laghman and Swat, and typically less V than those from Panjshir (Figure 15d; Guo *et al.* 2020; Krzemnicki *et al.* 2021; Chen *et al.* 2022).

DISCUSSION

The occurrence of quartz and mica inclusions in the Chitral emeralds is consistent with their geological setting in quartz- and mica-rich host rocks. Furthermore, the presence of inclusions of phlogopite as the main mica phase is consistent with the composition of the matrix rock (e.g. Figure 1 and the cover of this issue). By contrast, muscovite is the main mica inclusion in the Khaltaro samples. The plagioclase inclusions in the Chitral emeralds contain higher

Figure 15: Binary plots show element concentrations (obtained by LA-ICP-MS) for the emeralds of this study in comparison with data reported in the literature for emeralds from Panjshir, Laghman and Swat (Guo *et al.* 2020; Krzemnicki *et al.* 2021; Chen *et al.* 2022), as well as lighter-coloured Chitral samples analysed previously (Hanser *et al.* 2022). Error bars for Laghman and Panjshir emeralds show deviations from median values. (Sample Ye-11 from Guo *et al.* 2020 was excluded because Mg values of more than 220,000 ppm suggest that a mineral other than beryl was analysed.)

amounts of Ca (corresponding to andesine and oligoclase) than the albite in the samples from Khaltaro. The presence of muscovite and albite in the Khaltaro samples is consistent with their occurrence in hydrothermal veins rich in these minerals (Laurs *et al.* 1996). The general light green colour of the Khaltaro emeralds and their abundant inclusions, which also caused low transparency in our samples, have been noted in the literature (Lawrence *et al.* 1989). These characteristics limit their potential use as gemstones, although some clearer samples have been reported (Lawrence *et al.* 1989).

While usually of deep green colour, Swat emeralds are generally small and often included (Lawrence *et al.* 1989). This was also true for our Swat samples. The numerous dark inclusions may represent a variety of different minerals, and this contrasts with what we observed in our Chitral emeralds, in which phlogopite is the only dark inclusion present. Similarly, the biotite inclusions in Laghman emeralds differ from the phlogopite in Chitral emeralds.

Although two-phase inclusions were found in almost all the samples in this study, three-phase inclusions were absent from our Chitral emeralds. This is in contrast to our observations and the literature data on emeralds from Swat, Panjshir and Laghman, which all can contain three-phase inclusions. Nevertheless, it is possible that three-phase inclusions could rarely be encountered in Chitral emeralds in the future. The rectangular elongated and irregular shapes of the two-phase inclusions in Chitral emeralds resemble those of schist-hosted emeralds (Saeseaw *et al.* 2019).

The strong Fe^{2+} absorption at 830 nm in the UV-Vis-NIR spectra of our Chitral samples also identifies them as schist-hosted emeralds (Saeseaw *et al.* 2019), and thus distinguishes them from Swat and Panjshir emeralds, in which this feature is less pronounced or missing.

Raman spectroscopy in the E⊥c excitation showed a stronger type II H_2O peak than type I H_2O peak in samples from most localities examined for this study. The only exceptions were the specimens from Khaltaro, in which type I water was more pronounced regardless of the excitation direction. Since the presence of type II water correlates with alkalis in beryl (Wood & Nassau 1967; Aines & Rossman 1984; Mashkovtsev & Lebedev 1993; Fukuda & Shinoda 2008; Fukuda 2012), this indicates that the Chitral emeralds are alkali-rich (cf. Łodziński *et al.* 2005; Qiao *et al.* 2019) and contain more alkalis than those from Khaltaro. This was confirmed by chemical analyses, which showed less Na in the Khaltaro samples.

Chemical analyses revealed further differences among emeralds from the various localities. Compared to emeralds from Chitral, those from Swat have greater Mg, Na, Fe, Cr and Sc, but less Li and Cs. Thus, concentrations of these elements further distinguish these two localities, in addition to their differing UV-Vis-NIR spectra. Similarly, concentrations of Li, Na, Mg and Cs are lower in Panjshir emeralds than in our Chitral samples and can, therefore, help to differentiate between them.

More compositional overlap is seen among Khaltaro, Laghman and Chitral emeralds. Apart from lower Na and Mg contents, the lower V in Khaltaro emeralds may help distinguish them from Chitral emeralds. While Li is lower in Laghman emeralds than in those from Chitral, Cr is higher. Both elements may thus help distinguish Chitral from Laghman emeralds.

CONCLUSION

This follow-up study on deeper-coloured emeralds from Chitral in north-western Pakistan is largely in accordance with earlier observations of lower-quality stones from this deposit. In general, both the lighter- and darker-coloured samples exhibited similar spectra and chemical compositions, whereas some significant differences were found for emeralds from other localities in Pakistan and Afghanistan. This study confirms that the Chitral samples are alkali-rich, schist-hosted emeralds, which can thus be separated from Swat and Panjshir emeralds by their UV-Vis-NIR spectra and from Khaltaro emeralds also by their Raman spectra with E⊥c excitation.

Separation of Chitral from Laghman emeralds is less straightforward, since there can be considerable similarities in their spectra. Therefore, chemical analyses and inclusion observations are needed for their potential origin determination.

With the recent increase in emerald production from the Chitral region, distinguishing these emeralds from those of similar geological settings could become even more relevant and important in the near future.

REFERENCES

Aines, R.D. & Rossman, G.R. 1984. The high temperature behavior of water and carbon dioxide in cordierite and beryl. *American Mineralogist*, **69**(3–4), 319–327.

Aurisicchio, C., Conte, A.M., Medeghini, L., Ottolini, L. & De Vito, C. 2018. Major and trace element geochemistry of emerald from several deposits: Implications for genetic models and classification schemes. *Ore Geology Reviews*, **94**, 351–366, https://doi.org/10.1016/j.oregeorev.2018.02.001.

Bowersox, G., Snee, L.W., Foord, E.E. & Seal, R.R. 1991. Emeralds of the Panjshir Valley, Afghanistan. *Gems & Gemology*, **27**(1), 26–39, https://doi.org/10.5741/gems.27.1.26.

Chen, Q., Bao, P., Li, Y., Shen, A.H., Gao, R., Bai, Y., Gong, X. & Liu, X. 2022. A research of emeralds from Panjshir Valley, Afghanistan. *Minerals*, **13**(1), article 63, https://doi.org/10.3390/min13010063.

Deer, W.A., Howie, R.A. & Zussman, J. 2001. *Rock-Forming Minerals—Framework Silicates: Feldspars*, Vol. 4A, 2nd edn. The Geological Society, London, xii + 972 pp.

Fleet, M.E. 2003. *Rock-Forming Minerals—Sheet Silicates: Micas*, Vol. 3A, 2nd edn. The Geological Society, London, xxii + 758 pp.

Fukuda, J. 2012. Water in rocks and minerals – Species, distributions, and temperature dependences. *In*: Theophanides, T. (ed) *Infrared Spectroscopy – Materials Science, Engineering and Technology*. IntechOpen, London, 77–96, https://doi.org/10.5772/35668.

Fukuda, J. & Shinoda, K. 2008. Coordination of water molecules with Na^+ cations in a beryl channel as determined by polarized IR spectroscopy. *Physics and Chemistry of Minerals*, **35**(6), 347–357, https://doi.org/10.1007/s00269-008-0228-4.

Giuliani, G., Groat, L.A., Marshall, D., Fallick, A.E. & Branquet, Y. 2019. Emerald deposits: A review and enhanced classification. *Minerals*, **9**(2), article 105, https://doi.org/10.3390/min9020105.

Giuliani, G., Chaussidon, M., Schubnel, H.-J., Piat, D.H., Rollion-Bard, C., France-Lanord, C., Giard, D., de Narvaez, D. *et al.* 2000. Oxygen isotopes and emerald trade routes since antiquity. *Science*, **287**(5453), 631–633, https://doi.org/10.1126/science.287.5453.631.

Gübelin, E.J. 1982. Gemstones of Pakistan: Emerald, ruby, and spinel. *Gems & Gemology*, **18**(3), 123–139, https://doi.org/10.5741/gems.18.3.123.

Gübelin, E.J. & Koivula, J.I. 2008. *Photoatlas of Inclusions in Gemstones*, Vol. 3. Opinio Publishers, Basel, Switzerland, 672 pp.

Guo, H., Yu, X., Zheng, Y., Sun, Z. & Ng, M.F. 2020. Inclusion and trace element characteristics of emeralds from Swat Valley, Pakistan. *Gems & Gemology*, **56**(3), 336–355, https://doi.org/10.5741/gems.56.3.336.

Hagemann, H., Lucken, A., Bill, H., Gysler-Sanz, J. & Stalder, H.A. 1990. Polarized Raman spectra of beryl and bazzite. *Physics and Chemistry of Minerals*, **17**(5), 395–401, https://doi.org/10.1007/bf00212207.

Hammarstrom, J.M. 1989. Mineral chemistry of emeralds and some associated minerals from Pakistan and Afghanistan: An electron microprobe study. *In*: Kazmi, A.H. & Snee, L.W. (eds) *Emeralds of Pakistan*. Van Nostrand Reinhold, New York, New York, USA, 125–150.

Hanser, C.S., Häger, T., Botcharnikov, R. & Gul, B. 2022. Emerald from the Chitral region, Pakistan: A new deposit. *Journal of Gemmology*, **38**(3), 234–252, https://doi.org/10.15506/JoG.2022.38.3.234.

Henn, U. & Schmitz, F. 2014. Smaragde aus der Provinz Laghman, Afghanistan: Ein Vergleich mit Smaragden aus dem Panjshir-Tal. *Gemmologie: Zeitschrift der Deutschen Gemmologischen Gesellschaft*, **63**, 101–106.

Hu, Y. & Lu, R. 2020. Color characteristics of blue to yellow beryl from multiple origins. *Gems & Gemology*, **56**(1), 54–65, https://doi.org/10.5741/gems.56.1.54.

Huong, L.T., Häger, T. & Hofmeister, W. 2010. Confocal micro-Raman spectroscopy: A powerful tool to identify natural and synthetic emeralds. *Gems & Gemology*, **46**(1), 36–41, https://doi.org/10.5741/gems.46.1.36.

Karampelas, S., Al-Shaybani, B., Mohamed, F., Sangsawong, S. & Al-Alawi, A. 2019. Emeralds from the most important occurrences: Chemical and spectroscopic data. *Minerals*, **9**(9), article 561, https://doi.org/10.3390/min9090561.

Kazmi, A.H. 1989. A brief overview of the geology and metallogenic provinces of Pakistan. *In*: Kazmi, A.H. & Snee, L.W. (eds) *Emeralds of Pakistan*. Van Nostrand Reinhold, New York, New York, USA, 1–11.

Kazmi, A.H. & Snee, L.W. (eds) 1989. *Emeralds of Pakistan*. Van Nostrand Reinhold, New York, New York, USA, xii + 269 pp.

Khan, T. 1986. *Geology of the Pegmatite Belt in Chitral, Northwest Frontier Province, Pakistan*. Geological Survey of Pakistan Information Release 266, Quetta, Pakistan, 16 pp. + 5 maps.

Krzemnicki, M.S., Wang, H.A.O. & Büche, S. 2021. A new type of emerald from Afghanistan's Panjshir Valley. *Journal of Gemmology*, **37**(5), 474–495, https://doi.org/10.15506/JoG.2021.37.5.474.

Laurs, B.M., Dilles, J.H. & Snee, L.W. 1996. Emerald mineralization and metasomatism of amphibolite, Khaltaro granitic pegmatite-hydrothermal vein system, Haramosh Mountains, northern Pakistan. *Canadian Mineralogist*, **34**(6), 1253–1286.

Lawrence, R.D., Kazmi, A.H. & Snee, L.W. 1989. Geological setting of the emerald deposits. *In*: Kazmi, A.H. & Snee, L.W. (eds) *Emeralds of Pakistan*. Van Nostrand Reinhold, New York, New York, USA, 13–38.

Łodziński, M., Sitarz, M., Stec, K., Kozanecki, M., Fojud, Z. & Jurga, S. 2005. ICP, IR, Raman, NMR investigations of beryls from pegmatites of the Sudety Mts. *Journal of Molecular Structure*, **744–747**, 1005–1015, https://doi.org/10.1016/j.molstruc.2004.12.042.

Mashkovtsev, R.I. & Lebedev, A.S. 1993. Infrared spectroscopy of water in beryl. *Journal of Structural Chemistry*, **33**(6), 930–933, https://doi.org/10.1007/bf00745616.

Moroz, I.I. & Eliezri, I.Z. 1999. Mineral inclusions in emeralds from different sources. *Journal of Gemmology*, **26**(6), 357–363, https://doi.org/10.15506/JoG.1999.26.6.357.

Qiao, X., Zhou, Z., Schwarz, D.T., Qi, L., Gao, J., Nong, P., Lai, M., Guo, K. *et al.* 2019. Study of the differences in infrared spectra of emerald from different mining areas and the controlling factors. *Canadian Mineralogist*, **57**(1), 65–79, https://doi.org/10.3749/canmin.1800042.

Sabot, B., Cheilletz, A., de Donato, P., Banks, D., Levresse, G. & Barrès, O. 2001. The Panjsher-Afghanistan emerald deposit: New field and geochemical evidence for Colombian style mineralisation. *European Union Geoscience XI*, Strasbourg, France, 8–13 April, 548.

Saeseaw, S., Renfro, N.D., Palke, A.C., Sun, Z. & McClure, S.F. 2019. Geographic origin determination of emerald. *Gems & Gemology*, **55**(4), 614–646, https://doi.org/10.5741/gems.55.4.614.

Schmetzer, K. & Kiefert, L. 1990. Water in beryl – A contribution to the separability of natural and synthetic emeralds by infrared spectroscopy. *Journal of Gemmology*, **22**(4), 215–223, https://doi.org/10.15506/JoG.1990.22.4.215.

Schwarz, D. & Pardieu, V. 2009. Emeralds from the Silk Road countries – A comparison with emeralds from Colombia. *InColor*, No. 12, 38–43, http://www.incolormagazine.com/books/rxfa/#p=39.

Schwarz, D. & Curti, M. 2021. *Emerald – Modern Gemmology*. Bellerophon Gemlab, Bangkok, Thailand, 481 pp.

Snee, L.W., Foord, E.E., Hill, B. & Carter, S.J. 1989. Regional chemical differences among emeralds and host rocks of Pakistan and Afghanistan: Implications for the origin of emerald. *In*: Kazmi, A.H. & Snee, L.W. (eds) *Emeralds of Pakistan*. Van Nostrand Reinhold, New York, New York, USA, 93–123.

Wang, H., Shu, T., Chen, J. & Guo, Y. 2022. Characteristics of channel-water in blue-green beryl and its influence on colour. *Crystals*, **12**(3), article 435, https://doi.org/10.3390/cryst12030435.

Wood, D.L. & Nassau, K. 1967. Infrared spectra of foreign molecules in beryl. *Journal of Chemical Physics*, **47**(7), 2220–2228, https://doi.org/10.1063/1.1703295.

Zahid, M., Jan, M.Q. & Moon, C.J. 2016. Geochemistry of stratabound scheelite mineralisation and associated calc-silicate rocks from Chitral, NE Hindu Kush, Pakistan. *Arabian Journal of Geosciences*, **9**(13), article 620, https://doi.org/10.1007/s12517-016-2637-x.

The Authors

Carina S. Hanser FGA DGA*, **Dr Tobias Häger and Prof. Dr Roman Botcharnikov**
Institute of Geosciences, Johannes Gutenberg University Mainz, J.-J.-Becher-Weg 21, 55099 Mainz, Germany
and
Institute of Gemstone Research, Prof.-Schlossmacher-Straße 1, 55743 Idar-Oberstein, Germany
*Email: chanser@uni-mainz.de
https://orcid.org/0000-0001-5504-8739

Dr Tom Stephan
German Gemmological Association, Prof.-Schlossmacher-Straße 1, 55743 Idar-Oberstein, Germany

Bilal Gul
Department of Geology, University of Tartu, Ravila 14a, 50411 Tartu, Estonia